Experimental Investigation and Multi-Surface Failure Modeling of Fiber-Reinforced Adobe–Mortar Interfaces

Fatemeh Faghih Khorasani[1], Mohammad Zaman Kabir[2*], Farhang Farahbod[3], Khosrow Ghavami[4]

[1]Postdoctoral Researcher, Department of Civil and Environmental Engineering, Amirkabir University of Technology, Tehran, Iran

[2] Professor, Department of Civil Engineering, Amirkabir University of Technology, Tehran, Iran

[3]Assistant Professor, Road Housing and Urban Development Research Center, Ministry of Road and Urban Development, Tehran, Iran

[4] Professor, Department of Civil Engineering, Pontificia Universidade Catolica do Rio de Janeiro, Brazil

* mzkabir@aut.ac.ir

Abstract

Reliable modeling of adobe masonry requires material-specific characterization of the weak and highly variable adobe–mortar interface; however, experimentally calibrated interface failure envelopes for earthen masonry remain limited. This study presents a practical and systematic experimental–calibration procedure for characterizing adobe–mortar interaction under multiple stress states and translating the measured response into parameters suitable for numerical modeling. Four mortar configurations were investigated: plain mud mortar, mud mortar reinforced with tire-production waste fibers, and mud mortars reinforced with wheat straw fibers soaked for 10 min and one week. Direct tension, direct shear, compression, and combined compression–shear tests were conducted, and the results were represented by a unified multi-surface failure framework comprising a tensile cut-off, a frictional shear branch, and an elliptical compressive cap. Mortar composition and fiber condition affected both interface strength and the calibrated model parameters. The one-week-soaked straw mortar produced the highest mean measured strengths, with direct tensile, direct-shear, and compressive strengths of 0.040, 0.020, and 4.7 MPa, respectively, compared with 0.009, 0.008, and 3.5 MPa for plain mud mortar, while the fiber-containing mortars showed lower scatter than plain mud within the investigated three-specimen sets. The calibrated parameters are specific to the tested soil, materials, and loading protocol; nevertheless, the proposed procedure provides a transferable framework for the material-specific calibration of other earthen masonry systems. With validation across a broader range of soils, mortars, fiber conditions, and loading protocols, this approach could support comparative databases, design-oriented relationships, and the future development of technical guidance for adobe masonry interfaces.

Keywords: Adobe masonry; Adobe–mortar interface; Fiber-reinforced mud mortar; Experimental calibration; Multi-surface failure model; Interface failure envelope.

ACCEPTED MANUSCRIPT

1. Introduction

Growing concern over the environmental burden of conventional construction has renewed interest in locally available, low-processing materials. Earthen systems such as adobe, rammed earth, cob, and compressed earth blocks are attractive in this context because they can be produced with limited processing and can provide useful hygrothermal performance. Recent reviews also show that the behavior of earth-based materials depends strongly on soil composition, stabilization method, and fiber addition [1]. Their wider structural use, however, is still limited by low tensile and shear resistance, moisture sensitivity, drying shrinkage, and substantial material variability.

In adobe masonry, these limitations are not governed by the units alone. The mortar and, in particular, the unit–mortar interface can control cracking, sliding, and local loss of load transfer. Recent tests on adobe masonry have reported considerable scatter in compressive and shear response and have emphasized the importance of joint characterization in structural assessment [2]. Measured shear strength may also vary with specimen size and test configuration [3], which is relevant when experimental parameters are later used in analytical or numerical models.

Discrete fibers are commonly introduced into earthen materials to limit crack opening and improve post-cracking integrity. Their effect is not uniform: it depends on fiber type and geometry, moisture condition, dosage, surface characteristics, and the interaction with the soil matrix [4]. In earlier work on plain and short-fiber-reinforced clay adobes, fiber addition was also found to modify the compressive stress–strain response and the parameters needed for numerical simulation [5]. Recent work on straw-reinforced adobe similarly reports changes in mechanical, porosity, and hygrothermal behavior [6]. These findings support the use of fibers, but they also underline the need to evaluate each soil–fiber system on its own merits.

Recycled fibers offer a related approach while also making use of waste materials. Tire-derived fibers, for example, have been studied as reinforcement in soil-based composites [7]. Results obtained from bulk adobe or soil specimens, however, do not directly describe a masonry joint. At an interface, the response also depends on the surface condition of the unit, mortar shrinkage, local cracking, and the normal stress acting across the joint.

Masonry joints can fail through several mechanisms rather than a single strength limit. Interface opening or joint cracking may govern under low normal stress, while compression can activate frictional sliding, diagonal cracking, and eventually crushing. Multi-surface models were developed for conventional masonry to represent these mechanisms within one constitutive framework [8–10]. More recent meso-scale analyses of masonry built with earth mortar have reached a similar conclusion: cracking, shearing, and crushing at the interfaces all affect the predicted response, and the results are sensitive to the adopted interface parameters [11].

Most of these interface formulations were calibrated for fired brick, stone, or conventional mortars. Applying their parameters directly to adobe is questionable because earthen mortars are heterogeneous, shrinkage-sensitive, moisture-dependent, and weak in tension. Recent work on earthen mortar–brick interfaces has likewise shown the value of direct bond characterization rather than borrowing interface properties from conventional masonry [12].

ACCEPTED MANUSCRIPT

Experimental multi-surface envelopes for adobe–mud-mortar joints under tension, shear, compression, and combined loading are still comparatively limited.

Against this background, the present work examines four adobe–mortar systems: plain mud mortar, mud mortar with short tire-production waste fibers, and straw-fiber-reinforced mud mortars prepared with straw soaked for either 10 min or one week. Direct tension, direct shear, compression, and combined compression–shear tests were used to establish experimental points over different parts of the failure envelope.

The study therefore focuses on three related questions: how the interface responds under different stress states, how that response changes with mortar composition and fiber treatment, and whether the measured behavior can be represented by a common multi-surface framework. The resulting model combines a tensile cut-off, a frictional shear branch, and a compressive cap. The fitted values are specific to the tested materials and conditions; the broader contribution is the calibration procedure rather than a universal set of adobe-interface parameters.

2. Materials and Methods

The adobe units were produced using soil obtained from a local adobe-production workshop in the Tehran–Khatoonabad region, Iran. Particle-size analysis was carried out according to ASTM D2487, indicating approximately 90% clay and silt (particle size < 0.075 mm) and 10% sand (0.075–4.75 mm). According to ASTM D4318, the plastic limit, liquid limit, and plasticity index were 15, 23, and 8, respectively. XRD and XRF analyses were conducted as part of the original soil characterization. The available characterization record provides mineralogical-phase information rather than quantitative XRF oxide concentrations. Table 1 summarizes the principal mineralogical phases reported in this record, while the corresponding XRD pattern and peak list are provided in Appendix 1.

Table 1. Principal mineralogical phases reported for the investigated soil.

Identified compound	Chemical Formula	Mineral Name	Crystal System
Silicon Oxide	SiO_2	Quartz (low)	Trigonal
Calcium Magnesium Carbonate	$(Ca,Mg)CO_3$	Calcite, Magnesite	Rhombohedral
Calcium Aluminum Silicate	$CaAl_2Si_2O_8$	Anorthite	Triclinic
Aluminum silicate hydroxide	$Al_2Si_2O_5(OH)_4$	Kaolinite	Triclinic

Note: The chemical formulas identify the reported mineralogical phases and should not be interpreted as quantitative oxide contents expressed in wt.%.

The preparation procedure of the adobe blocks followed the methodology used in the authors' previous experimental work [13].

ACCEPTED MANUSCRIPT

The soil was mixed with the required water and left for 24 h to allow moisture penetration into remaining soil clods. The material was then thoroughly remixed and kneaded, placed and compacted in wooden molds, demolded, and air-dried under ambient laboratory conditions. After the initial drying period, the units were placed vertically to facilitate drying and were kept under ambient conditions for approximately one month.

The average dimensions of the adobe units were 50 × 200 × 50 mm^3, with an average mass of approximately 1150 g.

Four mortar types were considered: plain mud mortar, mud mortar reinforced with tire-production waste fibers, and mud mortars reinforced with wheat straw fibers soaked for either 10 min or one week. The two soaking durations were included to examine their effect on the measured macroscopic response.

Prepared mortars consisted of water and the same powdered soil used for the adobe units, with a nominal water content of approximately 40% relative to the dry-soil mass. The tire-production waste fibers were obtained directly from the Yazd Tire factory, Iran, and were used as received, without separation or additional treatment. Their nominal length was 10–30 mm. For the fiber-containing mortars, the prepared fibers were added at a bulk volume corresponding to 75% of the measured bulk volume of the wet soil. This 75% value represents the bulk-volumetric batching ratio used during specimen preparation and should not be interpreted as the true solid volume fraction of fibers in the mortar. Because the bulk volume of the wet fibers includes inter-fiber voids, this ratio cannot be directly converted to a conventional fiber volume fraction without additional measurements of fiber mass, moisture content, and bulk density/packing characteristics.

Composite specimens were constructed by bonding adobe units with the selected mortars. The same type of adobe unit was used throughout the program; the mortar-joint thickness was approximately 10 mm, and all specimens were cured for four weeks under the same environmental conditions.

Table 2 reports the nominal lengths of the fibers used in specimen preparation. The remaining values are literature-based reference properties for comparable fiber materials and are included only to provide general context regarding their typical orders of magnitude. These reference values were not measured for the specific fiber batches used in this study and were not used to calibrate the interface model.

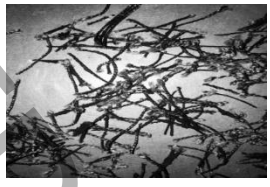
Representative views of the tire-production waste fibers and wheat-straw fibers used in specimen preparation are shown in Figure 1.

ACCEPTED MANUSCRIPT

Table 2. Nominal fiber lengths used in specimen preparation and literature-based reference properties of the fiber materials.

Property	Unit	Tire-production waste fiber	Wheat straw fiber
Nominal length used in this study	mm	10–30	10–40
Equivalent diameter (reference)	mm	0.80 [7]	Not measured
Tensile strength (reference)	MPa	600 [7]	14.7 [14]
Elongation at break (reference)	%	22 [7]	1.51 [14]
Elastic modulus (reference)	GPa	2.7 [7]	0.974 [14]
Water absorption (reference)	%	9.5 [7]	Approximately 300 [15]

(a)



(b)



Fig. 1. Fibers used in the experimental program: (a) tire-production waste fibers; and (b) wheat straw fibers.

3. Experimental Program

The testing program covered direct tension, direct shear, compression, and combined compression–shear loading. Together, these tests provided the experimental points used to define the tensile, frictional, and compressive portions of the failure surface.

Three nominally identical specimens were tested for each mortar and loading condition at approximately 22 °C and 55% relative humidity.

Loading was applied with a hydraulic jack mounted in a rigid frame and a load cell in series with the jack. A nominal loading rate of 10 kN/min was used throughout. Because rate sensitivity was not investigated independently, the measured strengths apply to this loading protocol and should not be treated as rate-independent properties. All four mortar configurations were tested under the same nominal procedure, allowing direct comparison.

ACCEPTED MANUSCRIPT

3.1. Adobe–Mortar Interface

A failure surface for an adobe–mortar interface should represent the distinct mechanisms that can govern masonry failure. Following Lourenço and Rots [8], these mechanisms include direct tensile cracking of the joints; sliding along bed or head joints at low normal stress; direct tensile splitting of the units; diagonal tensile cracking of the units under combined normal and shear stresses; and compressive failure associated with tensile splitting of the units due to mortar dilation at high compressive normal stress [16]. These mechanisms are illustrated schematically in Figure 2.

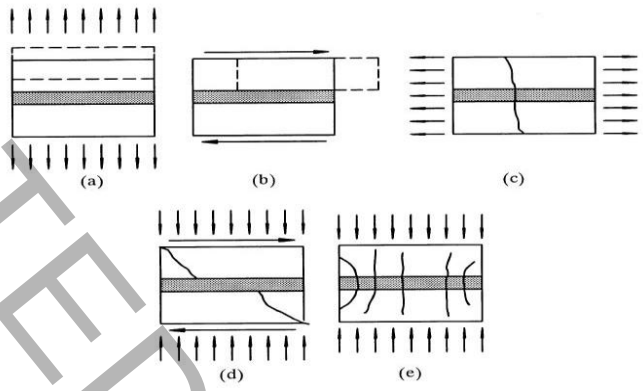


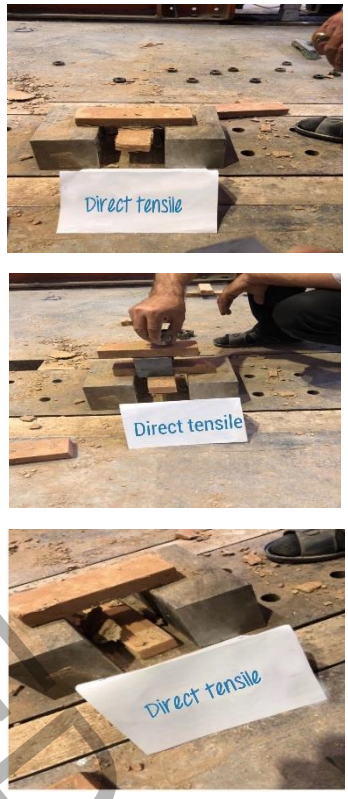
Fig. 2. Schematic masonry failure modes involving the unit–mortar interface: (a) direct tensile cracking of a joint; (b) sliding along a bed or head joint; (c) direct tensile cracking of a unit; (d) diagonal tensile cracking of a unit; and (e) masonry crushing [17].

Following the specimen concept reported in reference [18] and considering the low tensile resistance of the constituent materials, a small cross-shaped masonry specimen was used to promote approximately uniform tensile loading at the adobe–mortar interface (Figure 3). Load was increased continuously until tensile fracture of the mortar interface. For each specimen, the nominal tensile strength (f'_t) was calculated as follows:

$$f_t^{'} = \frac{P}{A} \tag{1}$$

where P is the ultimate load and A is the nominal bonded interface area (50 × 50 mm²). The results are reported in Table 3.

ACCEPTED MANUSCRIPT



(a)

(b)

(c)

Fig. 3. Direct-tension test of the adobe–mortar interface: (a) cross-shaped masonry specimen; (b) loading arrangement; and (c) tensile fracture along the mortar interface.

To determine the shear strength of the adobe–mortar interface, triplet masonry specimens were prepared following the general configuration of EN 1052-3 [19] and the setup described in [20]. Load was increased continuously to interface failure (Figure 4). The nominal shear stress at failure (τ_f) was calculated as follows:

$$\tau_f = \frac{P}{2A} \tag{2}$$

where P is the ultimate load and A is the nominal area of one bonded interface (50 × 200 mm²). The factor of two accounts for the two sheared interfaces in the triplet specimen. The results are reported in Table 3.

ACCEPTED MANUSCRIPT



(a)

(b)

(c)

Fig. 4. Direct-shear test of the adobe–mortar interface: (a) triplet masonry specimen; (b) loading arrangement; and (c) shear failure along the mortar interfaces.

To apply compression and shear simultaneously, a pair of steel loading devices was used in three oblique loading configurations (Figure 5), following the general setup concept reported in reference [21]. The configurations generated progressively different contributions of compressive normal stress and are designated LC-1, LC-2, and LC-3 in Table 3. At failure, the applied load was resolved into components normal and parallel to the bonded interface according to the geometry of the corresponding fixture.

For a bonded-interface area A, the stress components at failure were calculated as

$$|\sigma_{n,f}| = \frac{N_f}{A} \tag{3}$$

$$\tau_f = \frac{V_f}{A} \tag{4}$$

where N_f and V_f are the normal and parallel load components at failure, respectively. The nominal bonded-interface area was A = 200 × 50 mm². Table 3 reports the compressive normal-stress component as the positive magnitude $|\sigma_{n,f}|$ and the shear component as τ_f. In

ACCEPTED MANUSCRIPT

the model formulation, compression is negative; hence, the corresponding signed normal stress is $\sigma_n = -|\sigma_{n,f}|$.



(a) (b)

Fig. 5. Combined compression–shear test: (a) oblique loading fixture and specimen configuration; and (b) representative cracking before final failure (cracks highlighted in blue).

To estimate the interface compressive strength, specimens were constructed and tested as shown in Figure 6. Failure under compression was characterized by gradual development of limited vertical cracks on the lateral sides, followed by brittle failure. The nominal compressive strength (f'_c) was calculated as follows:

$$f'_c = \frac{P}{A} \tag{5}$$

where P is the ultimate load and A is the nominal loaded area (200 × 50 mm²).

(a) (b)

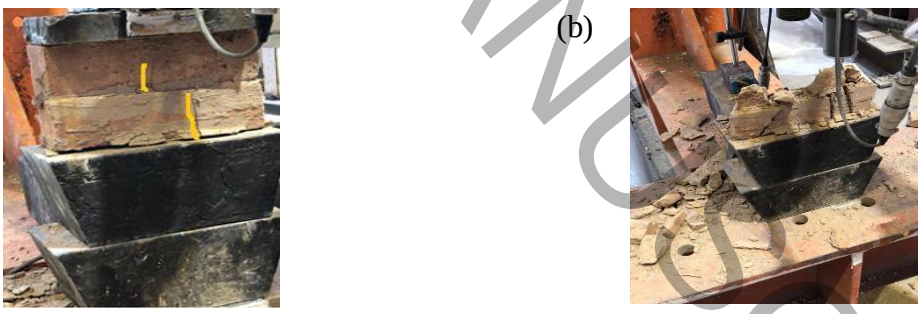


Fig. 6. Compression test: (a) test configuration and onset of vertical cracking (highlighted in yellow); and (b) brittle failure of the prism.

ACCEPTED MANUSCRIPT

Table 3. Mean interface strengths, combined-loading stress components, and coefficients of variation for the four mortar configurations (stresses in MPa).

Mortar	Direct tensile strength, f'_t	Direct shear strength, τ_f	**Combined compression–shear loading**						Compressive strength, f'_c (MPa)
			LC-1		**LC-2**		**LC-3**		
			τ_f	$\lvert\sigma_{n,f}\rvert$	τ_f	$\lvert\sigma_{n,f}\rvert$	τ_f	$\lvert\sigma_{n,f}\rvert$	
Plain mud	0.009	0.008	0.5	0.8	0.8	1.3	0.7	2.1	3.5
COV	40%	35%	40%	44%	42%	45%	48%	38%	44%
Mud + wheat straw fibers (one-week soaked)	0.04	0.02	1.2	1.6	1.8	2.4	1.4	3.4	4.7
COV	0.5%	0.2%	0.1%	0.5%	0.3%	0.2%	0.2%	0.2%	0.4%
Mud + wheat straw fibers (10-min soaked)	0.01	0.009	0.7	0.9	1	1.4	0.9	2.2	3.7
COV	0.4%	0.2%	0.4%	0.3%	0.5%	0.4%	0.2%	0.2%	0.3%
Mud + tire-production waste fibers	0.02	0.01	1.1	1.5	1.6	2.2	1.17	3	4
COV	0.3%	0.5%	0.5%	0.1%	0.4%	0.3%	0.5%	0.2%	0.2%

Note: LC-1, LC-2, and LC-3 denote the lower-, intermediate-, and higher-compression combined-loading configurations, respectively. For each configuration, τ_f is the shear stress

ACCEPTED MANUSCRIPT

at failure and $|\sigma_{n,f}|$ is the compressive normal-stress magnitude at failure. COV denotes coefficient of variation.

Each value in Table 3 is the mean of three specimens. The corresponding COV values provide descriptive measures of scatter among the replicate measurements. Scatter was higher for the plain mud mortar than for the fiber-containing mortars.

Representative bonded surfaces are shown in Figure 7. Plain mud joints exhibited more visible shrinkage cracks and discontinuities, whereas the fiber-containing joints were generally more continuous over the bonded area.

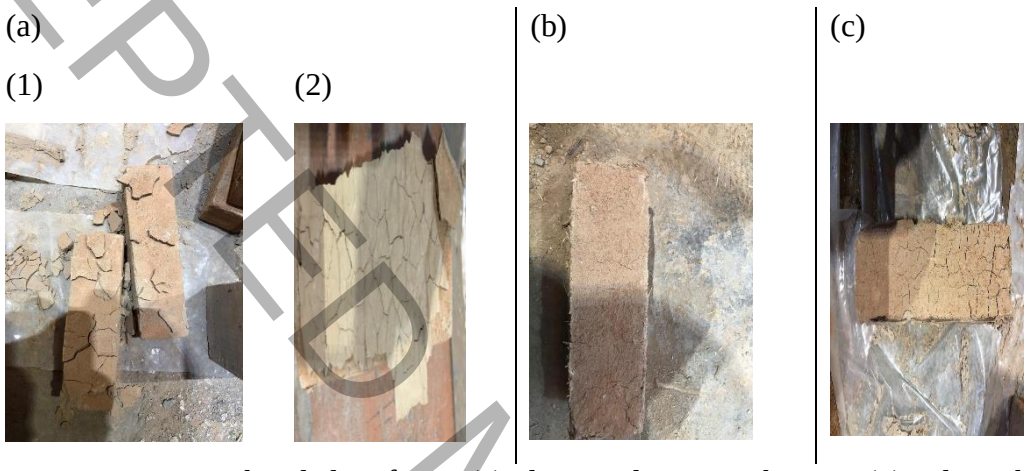


Fig. 7. Representative bonded surfaces: (a) plain mud mortar, showing (1) a deep shrinkage crack and (2) a shallow shrinkage crack; (b) straw-fiber-reinforced mud mortar; and (c) mud mortar reinforced with tire-production waste fibers.

4. Failure-Surface Formulation for the Adobe–Mortar Interface

An interface failure surface should represent the distinct tensile, sliding, combined-stress, and compressive mechanisms observed in masonry. A modified Mohr–Coulomb-type envelope with a small tensile cut-off has long been used to represent frictional materials and masonry-related failure behavior [22] (Figure 8). For masonry interfaces, multi-surface formulations have subsequently combined tensile cut-off and frictional sliding branches in different forms [8–10,23]. For example, Lourenço [10] adopted a vertical tensile cut-off, whereas alternative formulations have used inclined or zero-tension branches.

ACCEPTED MANUSCRIPT

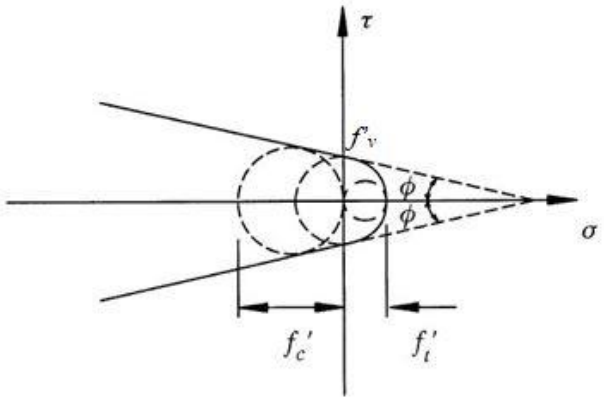


Fig. 8. Simplified failure envelope with a small tensile cut-off, adapted from [22].

Figure 9 schematically illustrates the vertical tensile cut-off and frictional branch used in the multi-surface representation; their quantitative calibration is described in Section 4.1.

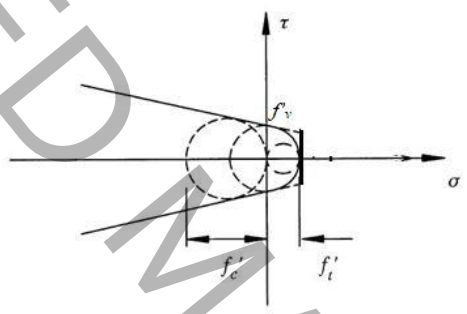


Fig. 9. Failure envelope with a vertical tensile cut-off and frictional branch.

Following the multi-surface interface framework developed for masonry [8,10], the high-compression failure region was represented by an elliptical cap that limits the admissible combinations of normal and shear stresses. The resulting interface failure surface consists of a tensile cut-off, a Coulomb-type frictional branch, and an elliptical compressive cap (Figure 10). For each branch, $f_i = 0$ defines the corresponding failure boundary, whereas $f_i < 0$ represents stress states within that boundary.

Normal stress σ_n is taken as positive in tension and negative in compression.

The three failure functions are defined as follows:

Tensile failure mode:

$$f_1(\sigma_n) = \sigma_n - f_t' \tag{6}$$

where f'_t is the tensile strength of the adobe–mortar interface.

ACCEPTED MANUSCRIPT

Shear failure mode

$$f_2(\sigma_n, \tau) = |\tau| + \sigma_n \tan\varphi - c \tag{7}$$

where c is the cohesion and φ is the friction angle.

Compressive-cap failure mode

$$f_3(\sigma_n, \tau) = C_{nn}\sigma_n^2 + C_{ss}\tau^2 + C_n\sigma_n - (f_c')^2 \tag{8}$$

where f'_c is the effective compressive strength obtained for the tested adobe–mortar assembly. The coefficient C_{nn} scales the contribution of normal stress, C_{ss} scales the contribution of shear stress, and the linear coefficient C_n controls displacement of the cap along the normal-stress axis.

Depending on the adopted interface formulation, the elliptical cap may be centered or non-centered (Figure 11).

In the present study, the centered-cap form was adopted with $C_{nn} = 1$ and $C_n = 0$, while tensile failure was represented separately by the tensile cut-off [8,10]. Equation (8) therefore reduces to:

$$f_3(\sigma_n, \tau) = \sigma_n^2 + C_{ss}\tau^2 - (f_c')^2 \tag{9}$$

Although compression corresponds to negative σ_n under the adopted sign convention, Table 3 reports compressive-stress magnitudes as positive values for readability. Defining the positive compression magnitude as $\sigma_c = -\sigma_n$, the Coulomb branch may equivalently be written as:

$$|\tau| = c + \sigma_c \tan\varphi \tag{10}$$

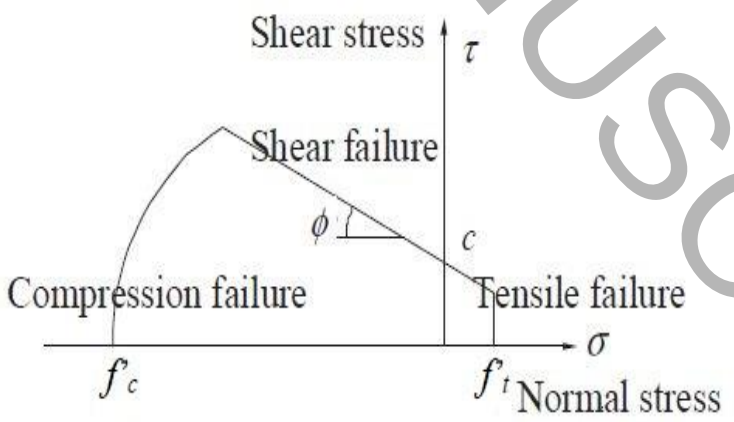


Fig. 10. Schematic multi-surface representation of the unit–mortar interface, adapted from the masonry interface framework in [8,10].

ACCEPTED MANUSCRIPT

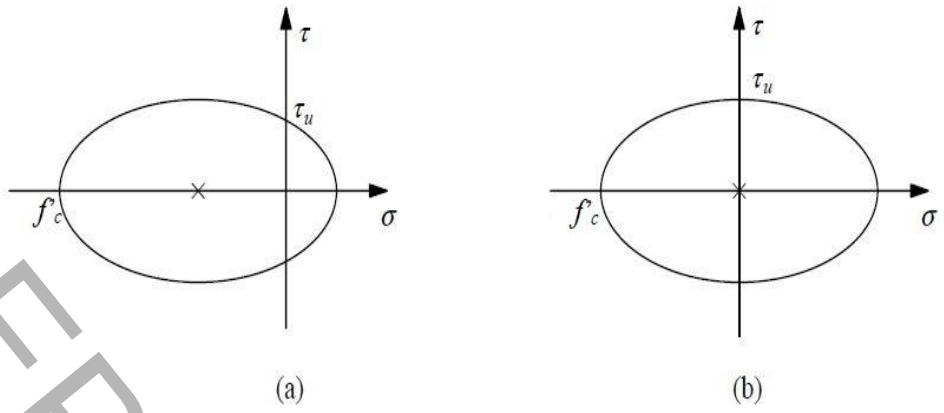


Fig. 11. Elliptical compressive-cap alternatives: (a) non-centered cap with different tensile and compressive intersections; and (b) centered cap with $C_{nn} = 1$ and $C_n = 0$, as adopted in this study.

4.1. Model Calibration

Calibration was based on the experimental values reported in Table 3. The direct-tension strength defined the tensile cut-off, while the direct-shear strength was used as cohesion c. The friction angle φ was fitted to the two lower-compression combined-loading points, LC-1 and LC-2, using $|\tau| = c + \sigma_c \tan \varphi$. The compressive cap was then fixed using the measured compressive strength f'_c together with the higher-compression point, LC-3. With the centered cap adopted here, LC-3 gives C_{ss} from Eq. (9).

A separate set of parameters was obtained for each mortar so that the effect of mortar composition could be compared directly.

The mortar is heterogeneous at the local scale because of porosity, shrinkage cracking, and nonuniform fiber distribution. For calibration, however, the joint was represented as an equivalent continuum. The fitted quantities should therefore be understood as effective interface parameters for the tested specimens rather than local material constants.

Table 4 lists the resulting effective parameters. Their interpretation should remain tied to this test series: only three specimens were available for each condition, and the calibration relies on the reported stress data in Table 3.

Table 4. Effective parameters of the calibrated multi-surface interface model.

Mortar	f'_t (MPa)	c (MPa)	φ (°)	f'_c (MPa)	C_{ss} (–)
Plain mud	0.009	0.008	31.4	3.5	16.00
Straw, one-week soaked	0.040	0.020	36.5	4.7	5.37
Straw, 10-min soaked	0.010	0.009	36.0	3.7	10.93
Recycled tire fiber	0.020	0.010	35.9	4.0	5.11

Note: φ was fitted using LC-1 and LC-2 with c fixed to the direct-shear strength; C_{ss} was obtained from LC-3 and f'_c. Compressive stresses are shown as positive magnitudes in this table.

ACCEPTED MANUSCRIPT

5. Results and Discussion

Figure 12 compares the final envelopes, each consisting of a tensile cut-off, a Coulomb-type frictional branch, and an elliptical compressive cap. The tensile and direct-shear strengths are much smaller than the compressive strengths; at the scale of the complete plots, these points therefore appear close to the origin.

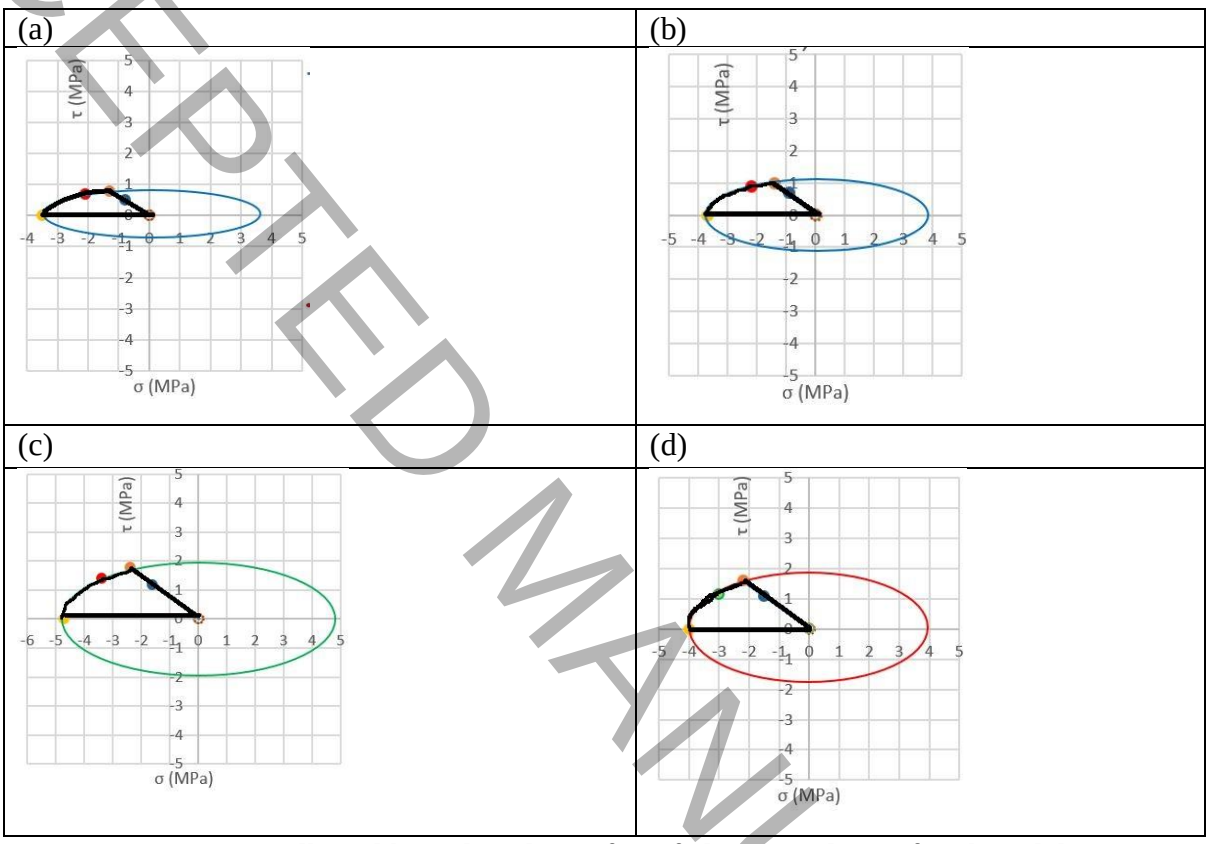


Fig. 12. Experimentally calibrated multi-surface failure envelopes for the adobe–mortar interfaces: (a) plain mud mortar; (b) mud mortar with 10-min-soaked straw fibers; (c) mud mortar with one-week-soaked straw fibers; and (d) mud mortar with tire-production waste fibers. Experimental points represent direct tension, direct shear, combined compression–shear loading, and compression. The direct tensile and direct shear points lie close to the origin because their magnitudes are substantially smaller than the compressive strengths.

Mortar composition affected both the magnitude and the repeatability of the measured interface strengths. In direct tension, the mean measured strength was 0.009 MPa for plain mud, 0.010 MPa for the 10-min-soaked straw mortar, 0.020 MPa for the tire-fiber mortar, and 0.040 MPa for the one-week-soaked straw mortar. The corresponding direct-shear strengths were 0.008, 0.009, 0.010, and 0.020 MPa, respectively. Compressive strength followed the same overall order, increasing from 3.5 MPa for plain mud to 3.7 MPa for the 10-min-soaked straw mortar, 4.0 MPa for the tire-fiber mortar, and 4.7 MPa for the one-

ACCEPTED MANUSCRIPT

week-soaked straw mortar. The combined compression–shear measurements showed the same general hierarchy. Thus, within the investigated test series, the one-week-soaked straw mortar produced the highest mean measured strength values across the reported loading conditions, while the tire-fiber mortar generally showed an intermediate response.

Within the three-specimen sets, the fiber-containing mortars exhibited lower scatter than plain mud. The more pronounced shrinkage cracks and discontinuities observed in some plain mud joints may have reduced the effective bonded area; however, this possible explanation was not verified by quantitative crack mapping or microstructural measurements.

The observed trends are broadly consistent with recent studies showing that fiber reinforcement can modify cracking behavior and mechanical response in earth-based composites [4,6]. Direct numerical comparison with other studies, however, should be made cautiously because the measured response depends on several material and testing variables, including soil mineralogy, fiber type and geometry, fiber dosage, moisture condition, curing procedure, specimen configuration, and loading method. The comparisons in the present study are therefore primarily intended to distinguish the four mortar configurations tested under the same experimental conditions.

The one-week-soaked straw mortar produced the highest mean strengths; however, the mechanism responsible for this improvement was not established experimentally. Pre-soaking may alter moisture exchange and drying-shrinkage behavior, increase fiber flexibility, or modify the soluble constituents released from the straw during soaking, any of which could influence fiber–matrix interaction and the resulting mechanical response. Internal curing is therefore considered only as one possible contributing mechanism rather than a demonstrated explanation. Microstructural and chemical characterization of the fiber–matrix transition zone would be required to distinguish among these mechanisms.

The tests also show why a single interface strength is not enough to describe these joints. Different parts of the response are governed by opening, frictional sliding under compression, and compressive failure. A composite envelope with a tensile cut-off, a Coulomb-type branch, and a compressive cap is therefore a useful representation. This is consistent with recent meso-scale modeling of earth-mortar masonry, where interface cracking, shearing, and crushing all affected the structural response [11], as well as with recent bond studies that argue for material-specific characterization of earthen interfaces [12].

The present interface-calibration framework complements the previously developed constitutive description of plain and short-fiber-reinforced adobe units [5]. Together, the two approaches allow the mechanical behavior of the adobe units and the unit–mortar interfaces to be characterized separately for future meso-scale numerical simulations.

The distinct calibrated envelopes demonstrate that mortar composition influences the effective interface parameters. However, the tested soil had a plasticity index of 8, and the calibrated parameters should therefore not be assumed to apply directly to soils with substantially different plasticity or clay mineralogy. Soils containing more active clay minerals or higher plasticity may exhibit different moisture sensitivity, drying-shrinkage behavior, and interfacial bonding. The proposed framework is therefore intended as a material-specific calibration procedure rather than a universal parameter set; its application to other soil–mortar systems requires recalibration under the relevant material and testing conditions. Reported scale and test-configuration effects in earthen-wall shear tests [3] further reinforce the importance of distinguishing between the model formulation and the calibrated parameter values. Applying the same tension, shear, compression, and combined-

ACCEPTED MANUSCRIPT

loading procedure to soils and mortars covering a broader range of material characteristics could support the development of a comparative database for material-specific design recommendations and, following broader validation, future code-oriented guidance.

6. Conclusions

This study investigated the mechanical response of adobe–mortar interfaces under direct tension, direct shear, compression, and combined compression–shear loading and used the experimental results to calibrate a multi-surface failure framework. Four mortar configurations were examined: plain mud, mud reinforced with short tire-production waste fibers, and straw-fiber-reinforced mud prepared using 10-min and one-week soaking periods.

The mortar configurations showed clear differences in interface strength. Direct tensile strength was 0.009, 0.010, 0.020, and 0.040 MPa for plain mud, 10-min-soaked straw, tire-fiber, and one-week-soaked straw mortars, respectively. The corresponding direct-shear strengths were 0.008, 0.009, 0.010, and 0.020 MPa, while compressive strength increased from 3.5 MPa for plain mud to 3.7, 4.0, and 4.7 MPa, respectively. The combined compression–shear results followed the same general trend. Thus, the one-week-soaked straw mortar produced the highest mean measured strength values among the investigated configurations, whereas the tire-fiber mortar generally showed an intermediate improvement. The fiber-containing mortars also showed lower scatter than plain mud within the three-specimen sets.

For all four mortars, the measured response could be represented by a composite failure envelope consisting of a tensile cut-off, a frictional shear branch, and an elliptical compressive cap. The differences among the calibrated envelopes demonstrate that mortar composition and fiber condition influence both the strength level and the effective interface parameters. The improved strength associated with one-week-soaked straw was experimentally observed, but its underlying mechanism was not established; therefore, moisture-related, shrinkage-related, and soaking-induced chemical effects should be regarded as possible explanations rather than confirmed mechanisms.

The proposed framework provides a practical procedure for characterizing and calibrating adobe–mortar interface failure surfaces for specific soil–mortar systems. Although the calibration procedure is potentially applicable to other earthen masonry systems, the parameter values obtained in the present study should not be directly generalized beyond the investigated soil, mortar compositions, and testing conditions. Broader experimental validation covering soils with different plasticity indices, clay mineralogies, and shrinkage characteristics is required to evaluate the transferability of the model formulation and to establish material-specific design guidance for earthen masonry interfaces.

ACCEPTED MANUSCRIPT

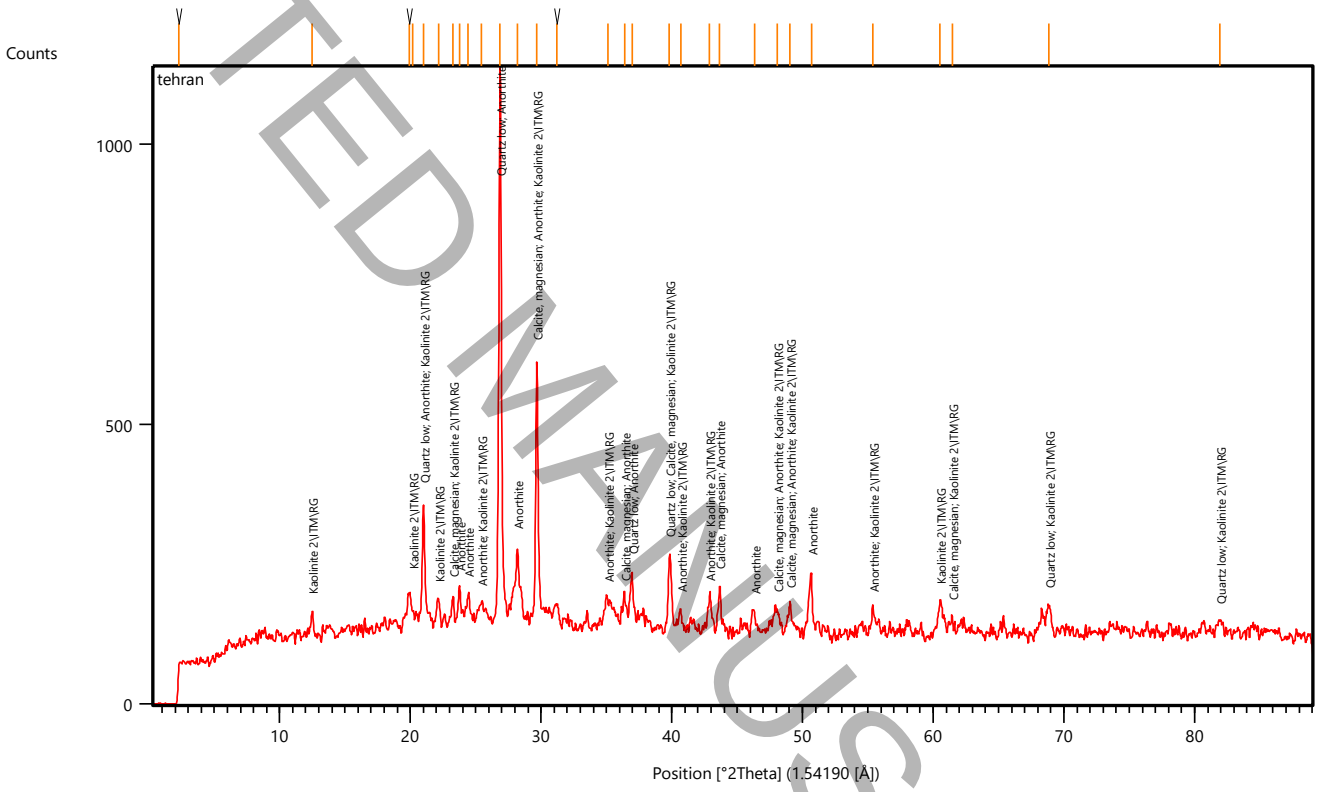
References

[1] V. Mora-Ruiz, J. Soto-Paz, S. Attia, C. Mejía-Parada, Sustainable Earthen Construction: A Meta-Analytical Review of Environmental, Mechanical, and Thermal Performance, Buildings, 15(6) (2025) 918.
[2] M.M. Rafi, S. Khan, M.A. Bhutto, Experimental Assessment of Compressive and Shear Behavior of Adobe Masonry, Journal of Materials in Civil Engineering, 36(6) (2024) 04024131.
[3] D.M. Ruiz, J.C. Reyes, Y.A. Alvarado, H. Vacca, N. Tarque, S. Jerez, Investigating Scale Effects on Experimental Shear Strength of Earthen Walls (Adobe and Rammed-Earth), Buildings, 15(5) (2025) 689.
[4] K. Saini, V.A. Matsagar, V.R. Kodur, Recent advances in the use of natural fibers in civil engineering structures, Construction and Building Materials, 411 (2024) 134364.
[5] F. Faghih Khorasani, M.Z. Kabir, K. Ghavami, A mathematical model for predicting complete compressive stress-strain curve of plain and short fiber reinforced clay adobes, AUT Journal of Civil Engineering, 5(1) (2021) 37–68.
[6] A. Alioui, S. Idrissi Kaitouni, Y. Azalam, N. Al Armouzi, E.M. Bendada, M. Mabrouki, Effect of straw fibers addition on hygrothermal and mechanical properties of carbon-free adobe bricks: From material to building scale in a semi-arid climate, Building and Environment, 255 (2024) 111380.
[7] M. Abbaspour, E. Aflaki, F. Moghadas Nejad, Reuse of waste tire textile fibers as soil reinforcement, Journal of Cleaner Production, 207 (2019) 1059–1071.
[8] P.B. Lourenço, J.G. Rots, Multisurface Interface Model for Analysis of Masonry Structures, Journal of Engineering Mechanics, 123(7) (1997) 660–668.
[9] N. Mojsilović, P. Marti, Strength of Masonry Subjected to Combined Actions, ACI Structural Journal, 94(6) (1997) 633–642.
[10] P.B. Lourenço, Computational strategies for masonry structures, PhD thesis, Delft University of Technology, Delft, 1996.
[11] Y. Endo, K. Miyoshi, Meso-scale numerical simulation of the mechanical behaviour of brick masonry in earth mortar, Journal of Building Engineering, 74 (2023) 106890.
[12] T. Zhang, J. Xue, C. Wu, Y. Sui, Y. Feng, Experimental and Finite Element Investigation of Bond Strength of Earthen Mortar–Brick Interfaces in Historic Masonry Structures, Buildings, 15(18) (2025) 3278.
[13] F. Faghih Khorasani, M.Z. Kabir, Experimental study on the effectiveness of short fiber reinforced clay mortars and plasters on the mechanical behavior of adobe masonry walls, Case Studies in Construction Materials, 16 (2022) e00918.
[14] M. El Messiry, R. El Deeb, Analysis of the Wheat Straw/Flax Fiber Reinforced Polymer Hybrid Composites, Journal of Applied Mechanical Engineering, 5(6) (2016) 240.
[15] M. Bouasker, N. Belayachi, D. Hoxha, M. Al-Mukhtar, Physical Characterization of Natural Straw Fibers as Aggregates for Construction Materials Applications, Materials, 7(4) (2014) 3034–3048.
[16] V.G. Haach, Development of a design method for reinforced masonry subjected to in-plane loading based on experimental and numerical analysis, PhD thesis, University of Minho, 2009.
[17] D.J. Sutcliffe, H.S. Yu, A.W. Page, Lower bound limit analysis of unreinforced masonry shear walls, Computers & Structures, 79(14) (2001) 1295–1312.
[18] R. van der Pluijm, Material properties of masonry and its components under tension and shear, in: Proceedings 6th Canadian Masonry Symposium, 15–17 June 1992, Saskatoon, Canada, University of Saskatchewan, 1992, pp. 675–686.

ACCEPTED MANUSCRIPT

[19] European Committee for Standardization (CEN), Methods of test for masonry – Part 3: Determination of initial shear strength, EN 1052-3:2002, CEN, Brussels, 2002.
[20] V. Alecci, M. Fagone, T. Rotunno, M. De Stefano, Shear strength of brick masonry walls assembled with different types of mortar, Construction and Building Materials, 40 (2013) 1038–1045.
[21] A. Kalali, M.Z. Kabir, Experimental response of double-wythe masonry panels strengthened with glass fiber reinforced polymers subjected to diagonal compression tests, Engineering Structures, 39 (2012) 24–37.
[22] W.F. Chen, D.C. Drucker, Bearing Capacity of Concrete Blocks or Rock, Journal of the Engineering Mechanics Division, 95(4) (1969) 955–978.
[23] A.W. Page, Finite Element Model for Masonry, Journal of the Structural Division, 104(8) (1978) 1267–1285.

Appendix 1



X-ray diffraction pattern of the raw material

The table of the peak list

Pos. [°2Th.]	Height [cts]	FWHM Left [°2Th.]	d-spacing [Å]	Rel. Int. [%]
2.2873	49.12	0.2519	38.64737	4.76
12.5076	42.53	0.1574	7.08116	4.12
19.9118	59.08	0.1889	4.46163	5.73
20.1738	71.31	0.0900	4.40187	6.91
21.0032	224.28	0.1574	4.23218	21.74

ACCEPTED MANUSCRIPT

22.1372	49.08	0.2519	4.01789	4.76
23.2767	56.57	0.1574	3.82371	5.48
23.7589	68.76	0.1574	3.74718	6.67
24.4351	58.73	0.2519	3.64501	5.69
25.4046	42.17	0.3779	3.50806	4.09
26.8567	1031.59	0.1574	3.32159	100.00
28.2135	144.27	0.1260	3.16487	13.99
29.6921	481.75	0.1574	3.01055	46.70
31.2379	40.15	0.3149	2.86501	3.89
35.0897	48.34	0.6298	2.55885	4.69
36.4042	54.08	0.2519	2.46942	5.24
36.9533	101.27	0.1260	2.43398	9.82
39.8241	133.99	0.2519	2.26489	12.99
40.6670	39.41	0.1889	2.21988	3.82
42.8758	60.55	0.1889	2.11050	5.87
43.6743	82.01	0.1260	2.07375	7.95
46.3181	39.52	0.2834	1.96135	3.83
48.0473	42.74	0.3779	1.89473	4.14
49.0353	50.77	0.1889	1.85884	4.92
50.6781	110.07	0.1889	1.80238	10.67
55.4001	41.75	0.1889	1.65942	4.05
60.5315	61.88	0.2519	1.53046	6.00
61.4487	30.63	0.3779	1.50980	2.97
68.8779	50.26	0.3149	1.36398	4.87
81.9214	20.14	0.3779	1.17669	1.95

ACCEPTED MANUSCRIPT